Local shear stress measurements on an axisymmetric body in a microbubble modified flow field

S. Deutsch and S. Pal
The Applied Research Laboratory and The Department of Mechanical Engineering, Pennsylvania State University, University Park, Pennsylvania 16804

(Received 18 May 1989; accepted 7 August 1990)

An array of flush-mounted hot film probes has been used to measure the local shear stress reduction as a result of microbubble injection over an axisymmetric body at the four discrete, free-stream speeds of 4.6, 10.7, 13.2, and 16.8 m/sec. Visualization of the bubble flow pattern supplement these results at intermediate free-stream speeds. At speeds of 10.7 m/sec and above, a circumferential gradient in skin friction, with skin friction reduction larger at the top than at the bottom of the model occurs at some distance downstream of injection. For these speeds, the gradient is stronger at the lower speeds and higher gas injection conditions. Higher speeds tend to drive the axial location of the gradient farther from the injection location. At speeds below 10.7 m/sec, the flow is dominated by a double vortex structure that entrains the bubbles at the bottom and sides of the model and transports them to the top. At sufficiently high gas flow rates a cavity, large enough to be observed visually, is formed just upstream of the vortices, centered near the body midline. The axial position of the cavity is roughly independent of flow speed and gas flow conditions. The transport of bubbles by the vortices, to the top of the body, is the cause of the poor skin friction reduction performance of microbubble injection at low speeds on an axisymmetric shape. Integration of the current local skin friction results gives good agreement with earlier drag balance measurements. The persistence of the drag reduction phenomenon with axial distance as well as the statistics of the shear stress fluctuations are quite similar to what was observed earlier on flat plates.

I. INTRODUCTION

The reduction of skin friction drag through the injection of gas, to form microbubbles into a liquid turbulent boundary layer, has received a good deal of experimental[1–4] and analytical/numerical[5–7] attention over the last 10 years. The decade's work was built on earlier studies by McCormick and Bhattarcharyya,[8] who used electrolysis to generate bubbles that reduced drag on a towed body of revolution, and by a group of Soviet researchers,[9–12] who observed microbubble drag reduction at low speeds on both a flat plate and in a pipe.

The most recent experimental studies[1–4] have characterized both the integrated and local skin friction reduction with microbubble injection for a flat plate[1, 2] and the integrated skin friction reduction for an axisymmetric geometry[4] at speeds as high as 18 m/sec. Both the trajectory of the microbubble cloud as well as some bubble size characteristics have also been studied.[3] The analytical/numerical studies,[5–7] which are all based on an assumption that the microbubble-laden boundary layer is a homogeneous medium with a spatially varying density and viscosity, have provided a first-order model for explaining the skin friction reduction phenomenon. A more detailed discussion of these studies may be found in a comprehensive review,[13] which has recently become available.

In the following, we shall only briefly discuss our current understanding of this drag reduction phenomenon. We note that this understanding is based, in general, on experiments and calculations made in zero pressure gradient, high-speed, turbulent boundary layers of typical laboratory dimensions.[13] It is clear from all the experimental studies that the injection of microbubbles can reduce the skin friction drag substantially for both flat plate and axisymmetric geometries. The primary nondimensional variable appears to be the ratio of gas to liquid volume flow rate in the boundary layer.[13] That is, in general, increasing the amount of gas volume relative to the amount of liquid volume in the boundary layer will increase the amount of drag reduction. Although useful, this normalization is less effective then we would like it to be in normalizing the data between different experiments and, moreover, it cannot explain the observed discrepancies between the effects of different gases.[4] Bubble sizes, as measured in a single study,[3] range from some ten times the sublayer thickness to a tenth of the boundary layer thickness. These values are apparently consistent with either a hypothesis that treats the bubble sizes as fixed by the injection process or one that treats bubble sizes as fixed by the turbulent energetics.[3, 13] No strong influence on the manner in which bubbles are injected has been observed.[8, 13] Based on trajectory measurements,[3] as well as analytical[6, 7] and numerical work,[5] it appears that the bubbles are most effective in reducing drag when they are near the buffer region. If fact, the abovementioned analytical and numerical work has sought to provide a first-order explanation of the phenomenon by postulating that the bubbles increase the viscosity near the buffer region, destroying some turbulent production scales there. Such a postulate ties the microbubble phenomenon to other near wall skin friction reduction techniques, such

 0899-8213/90/122140-07$02.00

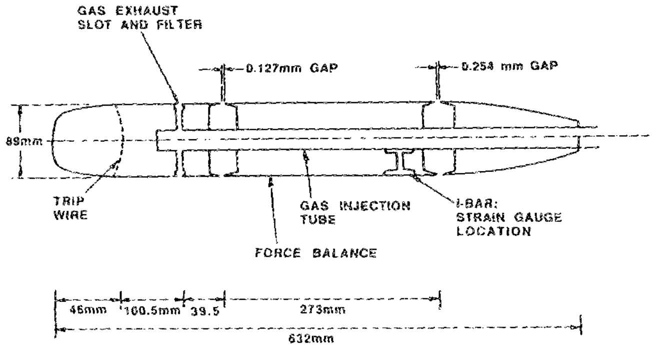

FIG. 1. The axisymmetric microbubble body.

TABLE I. Axisymmetric body.

Location from trip wire	U_∞ (m/sec)	R_θ	u^+ (m/sec)	y at $y^+ = 5$(μm)
155	5.26	2635	0.21	23.8
	10.71	5062	0.405	12.3
	16.94	8837	0.607	8.24
277	5.25	3491	0.21	23.8
	10.77	6764	0.406	12.3
	16.86	10 144	0.617	8.10
403	5.30	3775	0.210	23.8
	10.90	8191	0.413	12.11
	16.88	14 197	0.594	8.42

as polymer drag reduction. It was recently shown, in fact, that the microbubble and polymer shear stress statistics, as measured with flush mounted hot film probes, are similar at equivalent values of drag reduction.[14] An alternative interpretation, in which the mixing length is changed as a function of gas concentration, has been presented by Legner[6] and has predicted some of the measured data remarkably well.

It has also been observed that while the maximum value of drag reduction decreases with increasing speed on a flat plate over the speed range of 5–18 m/sec, it increases with increasing speed over roughly the same range for an axisymmetric body. An attempt to provide a physical explanation for this difference has been one motive for the current study. Here, we examine the local skin friction at a number of locations on an axisymmetric body, under the conditions of varying free-stream speed, gas flow, and gas type. These local skin friction measurement are supplemented by visual studies of the bubble cloud. The body used is that first employed for integrated skin friction measurements by Deutsch and Castano.[4] In addition to giving us an independent check on the earlier integrated skin friction results, the measurements of local skin friction gives us some understanding of the circumferential variation of skin friction. We have also been able to use this data, along with the flow visualization results, to help address the question of the variation of maximum skin friction reduction with free-stream speed. In particular, we are able to look more closely at the differing influence of buoyancy as a function of free-stream speed and body shape.

II. PROCEDURE

The experiments were run in the 12 in. diam water tunnel at the Applied Research Laboratory of the Pennsylvania State University. The model employed was that used by Deutsch and Castano[4] to measure the effect of microbubbles on the integrated skin friction drag. A schematic of the 89 mm diam, 632 mm long model is shown in Fig. 1. Gas is injected through a 6.35 mm long, 5.2 mm thick, cylindrical, sintered porous plastic section, which is located 146.5 mm downstream of the nose. The plastic material is rated as a 5 μm filter. A 0.35 mm diam steel wire was placed 46 mm downstream of the nose in an effort to ensure that fully developed turbulent boundary layers exist over the balance section for the free-stream velocities tested. Deutsch and Castano[4] characterized the no-gas-injection boundary layers using laser Doppler anemometry surveys at three locations on the balance (155, 277, and 403 mm downstream of the trip wire) and found that the boundary layer was indeed fully developed. In an effort to keep the current study self-contained, important boundary layer parameters are reprinted from Ref. 4, in Table I. Still more detail may be found in Ref. 4.

In the current experiment we obtained local skin friction data from an array of 12 flush-mounted hot film probes (TSI 1471W), which were placed on what had been the isolated force balance. Four probes were mounted on the horizontal and vertical axes of the model at each of the axial distances of 150 mm, 277 mm, and 403 mm from the trip wire. These three axial locations will henceforth be referred to as locations A, B, and C, respectively. Note that these locations correspond, as closely as the experimental geometry permitted, to the LDA measurement stations of Ref. 4. Additional circumferential locations were than obtained by rotating the balance section.

Calibration of the probes, which was based on the measured characteristics of the boundary layer,[4] was done *in situ* using a technique described in Ref. 2. Normally each data set contained local skin friction data from four probes at 10–15 values of gas flow rate and at constant free-stream speed. The data set was sandwiched between a pre- and post-test calibration. If the coefficient of the linear least-squares fit between these calibrations was less than 0.98, the entire data set was dropped. The data were A/D converted at 1000 Hz for 5 sec. Data acquisition and reduction was performed on a VAX 11/780 computer.

Data were taken for both air and helium injection. Circumferential injection uniformity was monitored visually. For some conditions, mirror image data about the vertical plane were available as a check on injection symmetry.

As in our earlier work, the free-stream velocity at the model was calculated by differencing the settling section pressure against the static pressure from a tap 213.5 mm from the nose of the body. Approach velocities were about 10% lower. Local skin friction measurements were made at speeds of 4.6, 10.7, 13.7, and 16.8 m/sec.

III. RESULTS AND DISCUSSION

In analyzing the skin friction reduction data with gas injection, for injection rates as high as 0.005 m^3/sec, we observed that the flow charcteristics for free-stream speeds greater than 10.7 m/sec were significantly different from those at free-stream speeds less than 10.7 m/sec. In particular, the flow field at the lower speeds was dominated by a twin vortex structure that entrained the gas bubbles and transported them, contained in the vortex core, to the top of the model. For the flow at the higher speeds, however, the bubble field was visually uniform. For this reason, we present the results in two separate sections.

As noted earlier, symmetry of the gas flow at injection was determined visually. In cases where mirror image data about the vertical plane was available, we have presented both values.

A. Local skin friction at speeds greater than 10.7 m/sec

The circumferential variation of skin friction drag ratio (C_f/C_{f_0}) is shown for both helium and air injection at a free-stream speed of 13.7 m/sec in Fig. 2. Data for low (0.001 m^3/sec), moderate (0.002 m^3/sec), and high (0.004 m^3/sec) gas injection rates are illustrated. As noted earlier, A, B, and C in the figure refer to probes mounted at axial stations 150, 277, and 403 mm from the trip ring. For each of these locations and at each of these gas flow rates, the ratio of the volume flow rate of gas to the volume of flow rate of gas and water in the boundary layer, $c_v = Q_A/Q_A + Q_W$, is also shown. This nondimensionalization of the gas flow rate has been found to be the best, to date, at correlating the available data.[13] Merkle and Deutsch[13] note the trajectories of the bubble cloud at different velocities are more nearly similar at constant values of volumetric flow ratio, c_v, and suggest that this is the reason that c_v is the best of the normalizations.

In Fig. 2, the decay of skin friction reduction with distance downstream is apparent. We observe from Figs. 2(a) and 2(b) that at low gas flow rates the skin friction reduction data for both air and helium injection are quite similar. For these flow rates skin friction reduction occurs only at the first axial station. Skin friction reduction is somewhat smaller at the bottom of the body than at the top. Furthermore, the skin friction reduction is larger at locations both above and below the horizontal plane through the centerline of the body. This suggests that the bubble cloud has split into two streams; one above and one below the centerplane.

At the moderate gas flow rate, the reduction has spread to the second axial station for both air and helium injection. Differences in skin friction between the two gases appears to be small. An interesting observation here is that although the reduction is still somewhat higher at the bottom of the model than at the top for the first axial station, a clear gradient in skin friction reduction—with the higher reduction on top—appears at the second axial station.

For the high gas injection rate, skin friction reduction is the order of 80%–90% at the first axial station and 60%–70% at the second axial station. A circumferential

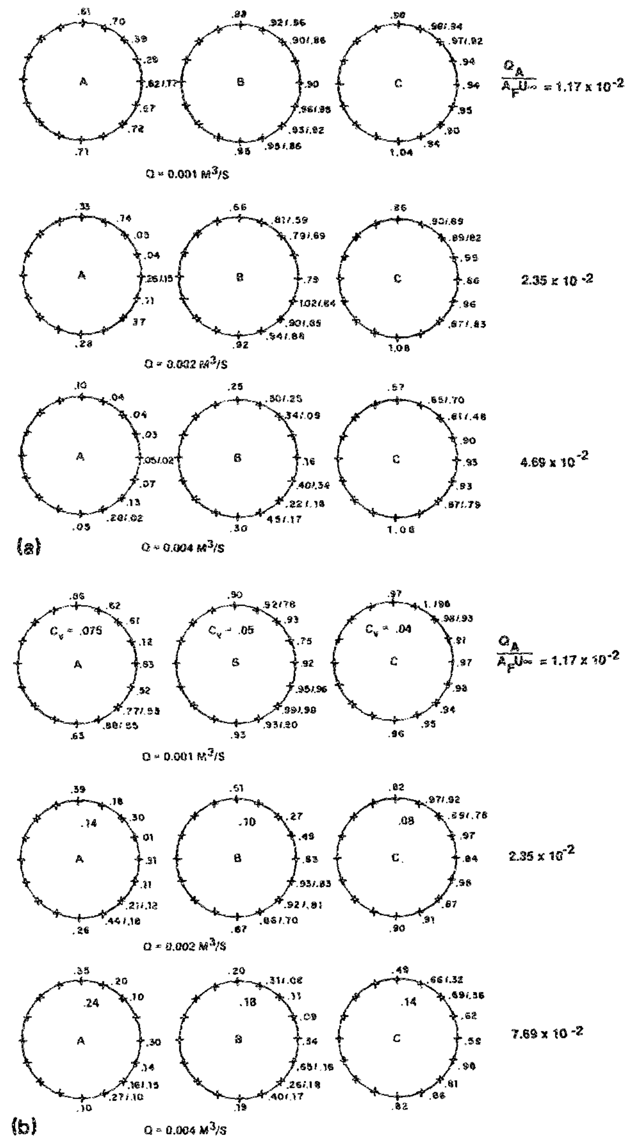

FIG. 2. Circumferential variation of skin friction ratio (c_f/c_{f_0}) for (a) air and (b) helium injection at a speed of 13.7 m/sec. The Reynolds number at the midpoint of the balance (R_L) is 3.8×10^6. The c_v values are the same in (a) and (b).

gradient in skin friction reduction, while no longer apparent at the second axial station, is now quite clear at the third. This suggests that the maximum skin friction reduction has been reached at the first two axial stations. Differences between the skin friction reducing effect of the two gases is within the scatter of the data. We shall find this to be true for the entire data set and shall therefore use either the air or the helium data interchangeably throughout the rest of the paper. The differences observed between helium injection and air injection, which we previously reported in Ref. 4, were at higher injection rates than we are reporting here.

Quite similar qualitative effects are seen at higher speeds. We illustrate this in Fig. 3 for the same three levels of air injection at a free-stream speed of 16.7 m/sec. Note that the levels of skin friction reduction are not as large here as for equivalent gas flow rates at 13.7 m/sec. (Note

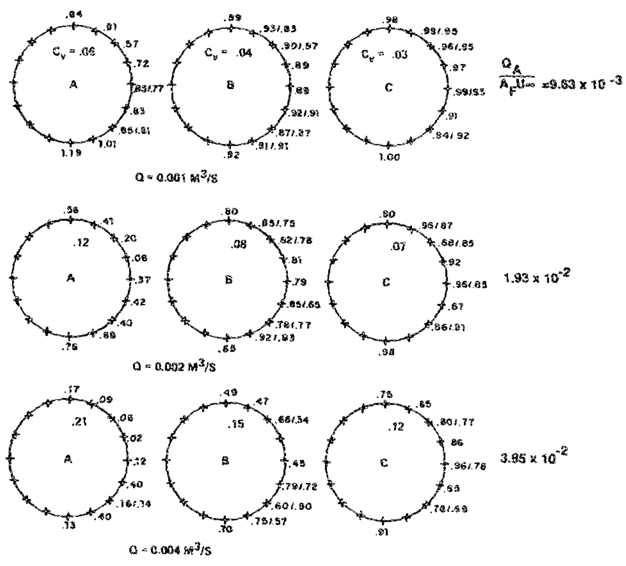

FIG. 3. Circumferential variation of skin friction ratio for air injection at a speed of 16.7 m/sec ($R_L = 4.6 \times 10^6$).

that larger skin friction reduction have been observed at 16.7 m/sec, particularly for helium injection. They were, however, at much higher gas flow rates than we consider here.) Moreover, the circumferential gradients in skin friction reduction values are only apparent for the highest gas flow rates (at axial stations B and C) and these gradients are not as strong. Maximum drag reduction has apparently only been achieved at the first axial station.

Finally, the data for 10.7 m/sec at the same three gas flow rates (helium here), which we present in Fig. 4, again give the same qualitative pattern of skin friction reduction. Here, however, we see a very high level of skin friction reduction for moderate and high gas flow rates and very

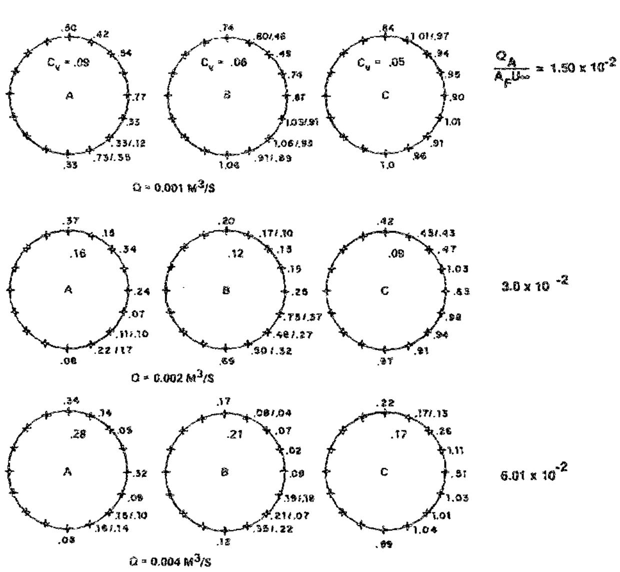

FIG. 4. Circumferential variation of skin friction ratio for helium injection at a speed of 10.7 m/sec ($R_L = 2.9 \times 10^6$).

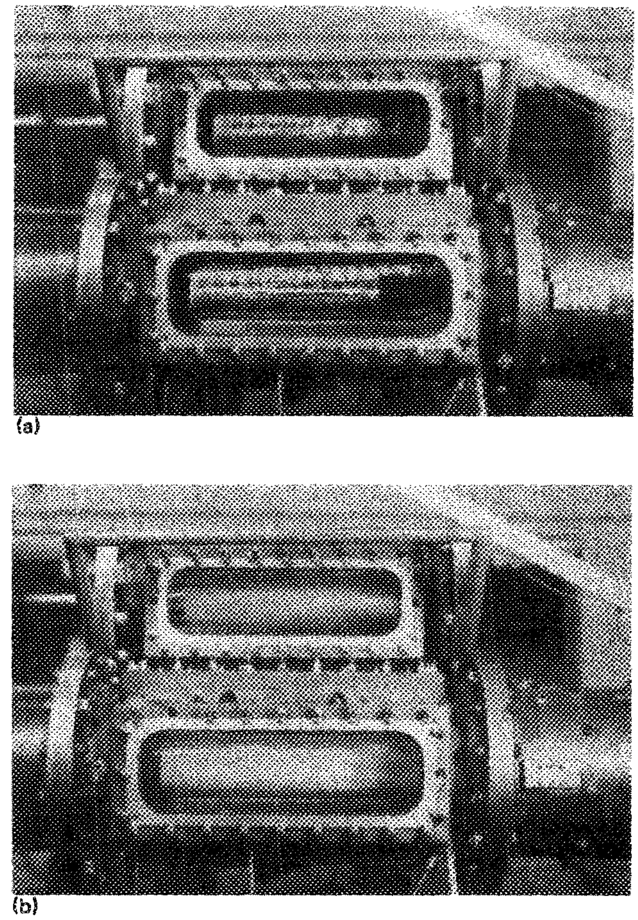

FIG. 5. Photograph of the two states of the microbubble flow field. The photograph at the top is at a speed of 4.6 m/sec ($R_L = 1.3 \times 10^6$), while that at the bottom is at a speed of 16.7 m/sec ($R_L = 4.6 \times 10^6$). The airflow rate is 0.004 m^3/sec. At the midpoint of the balance, c_v is 0.33 for the top photograph and 0.15 for the bottom.

strong circumferential skin friction gradients. At the high gas flow rate, saturation of the drag reduction is again apparent at the first and second axial stations.

The formation of a gradient in skin friction reduction, with larger reductions at the top of the body, requires that more boundary layer gas be at the top than the bottom of the model as the axial distance from the injection location increases. A general lift up of the bubble cloud with increasing axial distance is the most likely cause of this phenomenon. The variation of both the strength of the gradient and the apparent axial location of the gradient with free-stream speed and gas flow rate is consistent with this argument.

B. Local skin friction variation at speeds below 10.7 m/sec

At low free-stream speeds, the flow is dominated by the formation of two intense vortices, which carry bubbles from the bottom of the model to the top. A photograph of the vortex flow, taken at a free-stream speed of 4.7 m/sec and a gas flow rate of 0.004 m^3/sec is shown in Fig. 5. Also shown in Fig. 5 is a photograph of the microbubble flow field for a higher speed, but equivalent airflow rate, at which the vortices are not present.

The formation of these vortices, as determined visually, is at a gas flow rate of 0.001 m^3/sec for a free-stream speed of 4.6 m/sec and a gas flow rate of 0.002 m^3/sec for a speed of 7.6 m/sec. We have found that these vortices do appear at higher free-stream speeds also, but for gas flow rates that are larger than those at which we normally test. Formation of the vortices with increasing gas flow rate is, as observed visually, an abrupt transition in the nature of the flow. Once formed the vortical structures maintain the same axial location as the gas flow rate is increased, although the structure appears to intensify. By this we mean that the gas from an increase in gas flow rate is also completely entrained. The axial location at which these vortices form does not appear to vary much with free-stream speed. For large gas flow rates, we observe the formation of a gas cavity just upstream of the vortical structure, centered at about the body centerline. Such a cavity formation has been previously documented by workers concerned with, among other problems, the nature of the boundary layer on a missile entering a liquid.[15]

The reaction of the hot film probes to the changing flow field is given in Fig. 6. Here positions 1 and 2 are near the top of the body, 3, 4, and 5 at the side, and 6 at the bottom. At the first axial station the increase in skin friction reduction with increasing gas flow rate is typical of what we have observed in the flat plate data. At the second axial station, however, only the probes at the top of the body are seeing skin friction reduction—and hence boundary layer gas. The probes at the bottom and sides see an initial return to no skin friction reduction followed by a skin friction increase with a continued increase in gas flow rate. We believe that this increase in skin friction, above its no injection value, is due to the acceleration of the fluid around the separated flow of the cavity region. The data at the third axial station is similar, except that the region of skin friction reduction is now confined to the very top of the body, which corresponds to the narrowing of the vortex core, and the acceleration of the flow about the cavity is lessened as the flow relaxes.

The twin vortex formation and the consequent elimination of boundary layer gas over much of the area of the body is the apparent cause of poor microbubble skin friction reduction performance on axisymmetric bodies at low speeds. As the free-stream speed is increased, the increased convection of bubbles and the decreased ratio of gas to water flux in the boundary layer delays the onset of the instability. One might speculate then that the mechanism for the formation of these vortices is associated with "buildup" of gas at some flow location. A gravitational-(Richardson)-type instability would seem the most likely cause of the vortex formation.

C. Comparison with earlier results

Simple circumferential and axial averaging of the local skin friction data allows us to compare it against the integrated skin friction data presented in Ref. 4, and to compare the persistence of the axisymmetric data with earlier flat plate results presented in Ref. 2.

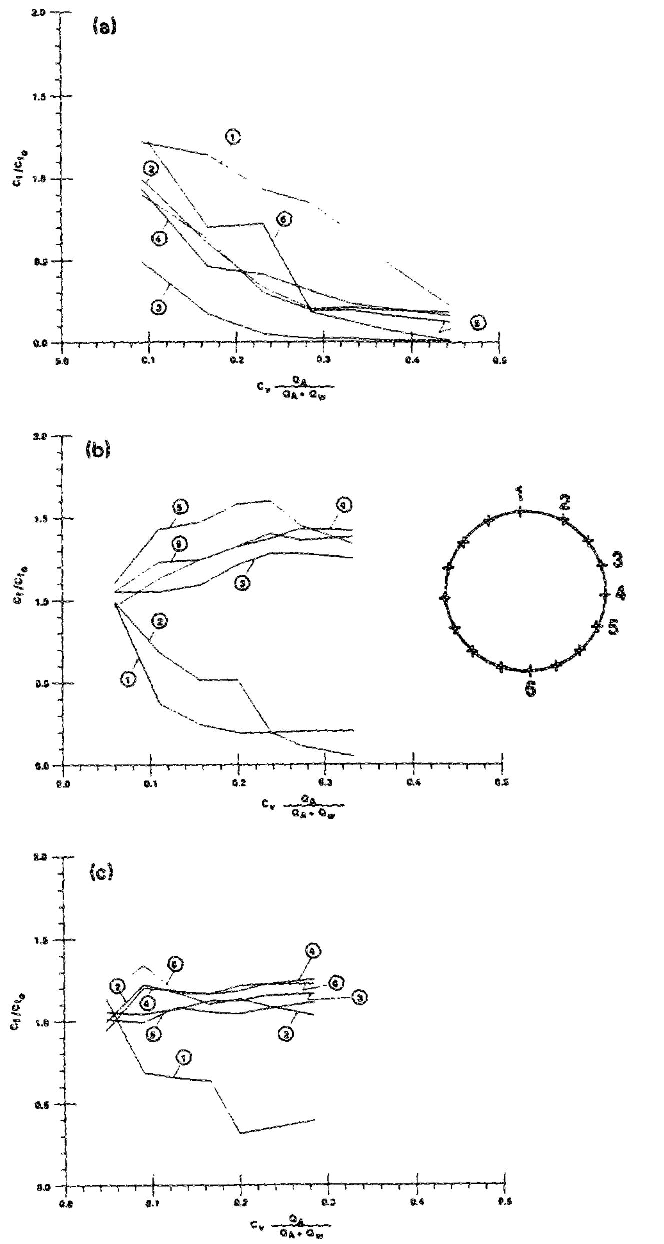

FIG. 6. Response of the hot film probes to the vortex flow field. The velocity is 4.6 m/sec ($R_L = 1.3 \times 10^6$) and helium is being injected. Here (a), (b), and (c) are located, respectively, 155, 277, and 403 mm downstream of the trip wire.

A comparison of the averaged local measurements against the drag balance data is shown in Fig. 7. The comparison, which is shown for several free-stream speeds, is good. A plot of the persistence of the skin friction reduction is shown in Fig. 8. The axial distance between positions A and C is roughly 30–40 boundary layer thicknesses, so that the persistence of the phenomenon on an axisymmetric body, for the conditions for which the vortical structures do not arise, appears to be the same order of magnitude as that observed for the flat plate.[2]

The shear stress fluctuation statistics are also similar to those that we have previously observed on a flat plate.[2,14]

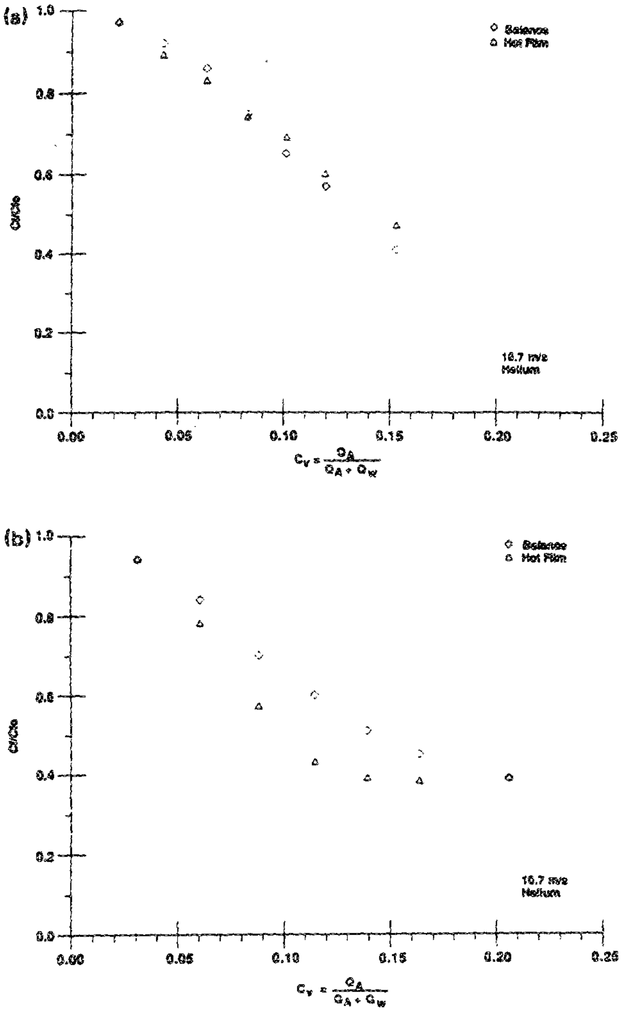

FIG. 7. Average of the local skin friction results versus the integrated drag balance results. (a) is at a speed of 16.7 m/sec ($R_L = 4.6\times10^6$) while (b) is for a speed of 10.7 m/sec ($R_L = 2.9\times10^6$). Helium is being injected.

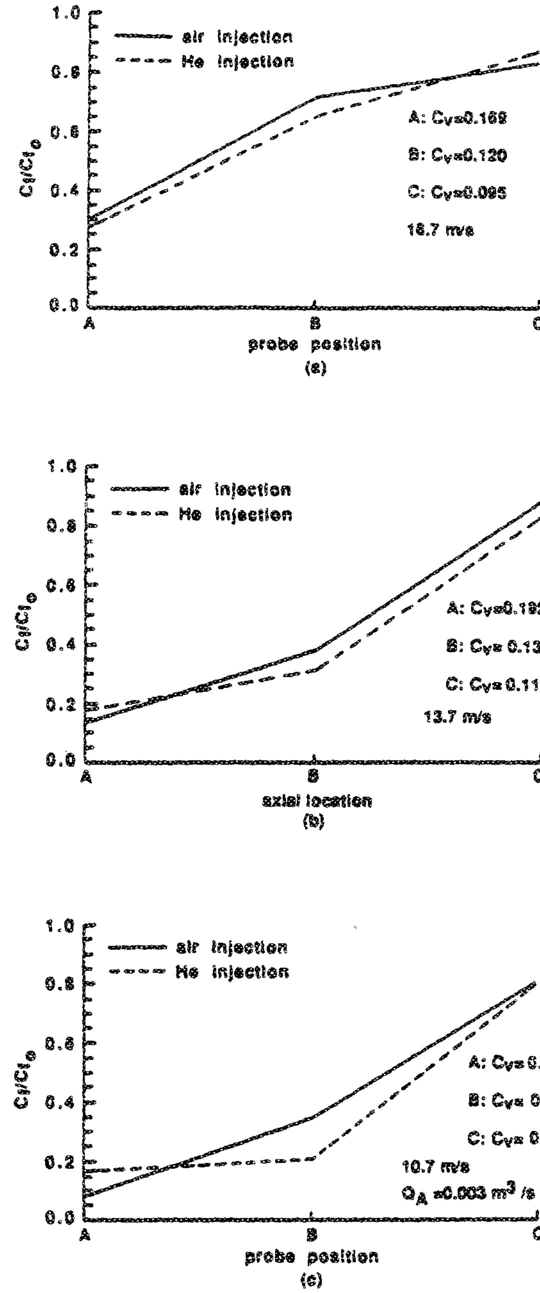

FIG. 8. Persistence of the drag reduction with axial distance. (a) is for a speed of 16.7 m/sec ($R_L = 4.6\times10^6$), (b) a speed of 13.7 m/sec ($R_L = 3.8\times10^6$), and (c) a speed of 10.7 m/sec ($R_L = 2.9\times10^6$). The gas flow rate is 0.003 m^3/sec.

In Fig. 9, we compare results for the normalized turbulent intensity, skewness and kurtosis of the shear stress fluctuations for the axisymmetric body against those taken earlier on a flat plate at equivalent values of drag reduction.[14] We find a very large increase in the values of the higher moments for drag reductions of greater than about 40%. The spectrum (not presented here) of the shear stress signals also suggest, that like the flat plate data, there is an increasing loss of high frequency fluctuations with increasing gas flow rate. These results suggest that the influence of the bubbles on the turbulence characteristics is similar, at equivalent values of drag reduction, for both geometries and that the nature of this turbulence is changing for values of drag reduction higher than about 40%. Quite similar results have been shown for polymer injection in Ref. 14.

IV. CONCLUSIONS

One of the more serious inconsistencies in microbubble research has been the differing behavior of maximum drag reduction with changing free-stream speed for flat plates and axisymmetric shapes. We had previously found that for flat plate flows, at speeds above 5 m/sec where buoyancy ceases to dominate, maximum drag reduction decreases for increasing free-stream speed,[1,2] while the opposite behavior had been observed on axisymmetric bodies.[4] In the current study we show that the poor behavior of microbubbles in reducing drag at speeds below 10.7 m/sec is due to the formation of twin vortices that capture and convect the boundary layer gas to the top of the body. Once these twin vortices form, additional gas flow rate is not productive, as it is also entrained. At sufficiently high gas flow rates a visible gas cavity is formed upstream of these vortices. At speeds above 10.7 m/sec, the increased

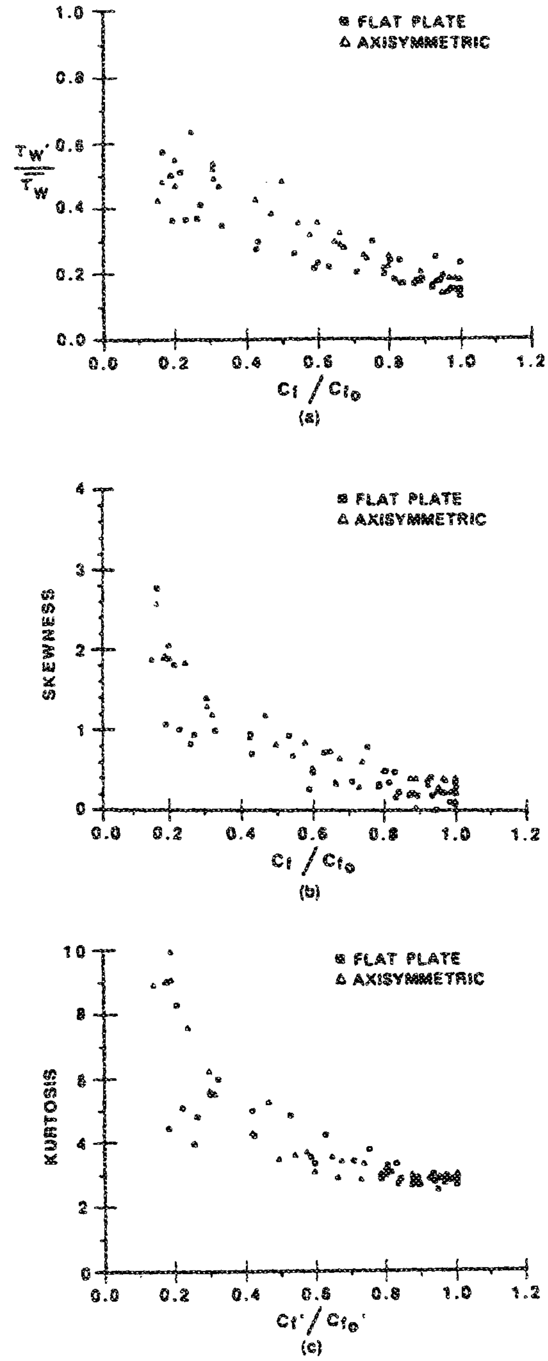

FIG. 9. Comparison of the shear stress fluctuation statistics between the axisymmetric and the flat plate geometries. (a) gives the intensity, (b) the skewness, and (c) the kurtosis.

convection and smaller bubble sizes produce a bubble cloud that is thinner and more confined to the wall region.[3] These conditions tend to suppress the vortex formation until gas flow rates are reached that are larger than those we normally test at.

We have speculated that the onset of the twin vortices might be caused by a density gradient in the vertical direction. Such a density gradient can arise because of the axisymmetric shape. Bubbles above the horizontal centerplane are free to rise, while those below are constrained to some extent by the presence of the body. As the bubble cloud grows with increasing gas flow rate, its extent may become much larger than the boundary layer region of large velocity gradients and a Richardson-type instability could arise. We might speculate further, on the basis of the high speed data that does not show this vortex formation, that the instability would occur at some gas flow rate higher than that required for saturation of the drag reduction at a position upstream of the vortex location.

A reviewer has suggested that the onset of the vortex formation might scale as the ratio of the gas flow rate per unit frontal area of the body to the flow speed. Values for this parameter are given in Figs. 1–4. For this parameter to be successful, however, the gas flow rate at onset must scale as the velocity. We do not find this to be the case. Onset at 15 m/sec, for example, requires much more than twice the gas flow at 7.5 m/sec. As implied by the comments of the reviewer, however, it would appear to be of interest to study the onset for axisymmetric bodies of different radii.

The existence of a vortex state in which microbubbles are not effective in reducing drag will complicate the already difficult problem of scaling the phenomenon to other model sizes and shapes and other ranges of speed. Although detailed theoretical or numerical studies for dense interacting bubble clouds are not yet possible, phenomenological models that employ the variable properties of a homogenous fluid model might lead to a better understanding of the overall dynamical behavior of the twin vortical structure.

ACKNOWLEDGMENTS

Conversations with Professor Merkle, Professor Billet, and Professor Petrie have been very helpful.

This work was supported under ONR Contract No. N00014-87-K-0196 under the supervision of Mr. J. Fein.

[1] N. K. Madavan, S. Deutsch, and C. L. Merkle, Phys. Fluids **27**, 351 (1984).
[2] N. K. Madavan, S. Deutsch, and C. L. Merkle, J. Fluid Mech. **156**, 237 (1985).
[3] S. Pal, C. L. Merkle, and S. Deutsch, Phys. Fluids **31**, 744 (1988).
[4] S. Deutsch and J. Castano, Phys. Fluids **29**, 3590 (1986).
[5] N. K. Madavan, C. L. Merkle, and S. Deutsch, J. Fluid Eng. **107**, 370 (1985).
[6] H. H. Legner, Phys. Fluids **27**, 2788 (1984).
[7] J. L. Marie, J. PhysicoChem. Hydrodyn. **13**, 213 (1987).
[8] M. E. McCormick and R. Bhattacharyya, Nav. Eng. J. **85**, 11 (1973).
[9] G. S. Migirenko and A. R. Evseev, *Problems of Thermophysics and Physical Hydrodynamics* (Nauka, Novosibirsk, 1974) (in Russian).
[10] Yu. N. Dubnishchev, E. R. Evseev, V. S. Sobolev, and E. N. Utkin, J. Appl. Mech. Tech. Phys. **16**, 114 (1975).
[11] V. G. Bogdevich and A. G. Maluga, in *Investigations of Boundary Layer Control*, edited by S. S. Kutateladze and G. S. Migirenko (Thermophysics Institute, Novosibirsk, 1976), p. 62 (in Russian).
[12] V. G. Bogdevich and A. R. Evseev, in Ref. 10, p. 49.
[13] C. L. Merkle and S. Deutsch, in *Frontiers in Experimental Fluid Mechanics*, edited by M. Gad-el-Hak (Springer, Berlin, 1989), pp. 291–335.
[14] S. Pal, S. Deutsch, and C. L. Merkle, Phys. Fluids A **1**, 1360 (1989).
[15] R. N. Cox and W. A. Clayden, *Cavitation in Hydrodynamics*, Proceedings of a Symposium at the Naval Postgraduate Laboratory, Report 12, 1955.